

New Interpenetrated Copper Coordination Polymer Frameworks having Porous Properties

Prakash Kanoo,[†] Ryotaro Matsuda,^{‡,§} Masakazu Higuchi,[⊥] Susumu Kitagawa,^{‡,§,⊥}
and Tapas Kumar Maji^{*,†}

[†]Molecular Materials Laboratory, Chemistry and Physics of Materials Unit, Jawaharlal Nehru Centre for Advanced Scientific Research, Jakkur, Bangalore 560 064, India, [‡]Kitagawa Integrated Pore Project, ERATO, JST, Kyoto Research Park, Building 3, Shimogyo-ku, Kyoto 600 8815, Japan, [§]Institute for Integrated Cell-Materials Sciences (iCeMS), Kyoto University, 69 Konoe-cho, Yoshida, Sakyo-ku, Kyoto, Japan, and [⊥]Department of Synthetic Chemistry and Biological Chemistry, Graduate School of Engineering, Kyoto University, Katsura, Nishikyo-ku, Kyoto 615 8510, Japan

Received August 20, 2009

Two new 3-fold interpenetrated 3D microporous metal-organic coordination polymers (MOCPs) of Cu(II), [Cu₃(bipy)_{1.5}(2,6-ndc)₃]_n (**1**) and {[Cu(bpe)_{0.5}(2,6-ndc)]·0.5H₂O}_n (**2**) (bipy = 4,4'-bipyridine; bpe = 1,2-bis(4-pyridyl)ethane; and 2,6-ndc = 2,6-naphthalenedicarboxylate), have been synthesized using a mixed-ligand system and structurally characterized by single-crystal X-ray diffraction study. Room-temperature reaction of Cu(II) with bipy and 2,6-ndc affords **1**, whereas reaction with bpe and 2,6-ndc yields **2**. Structure determination reveals that in both cases, a 2D square grid made by Cu(II) and 2,6-ndc with the aid of Cu₂(CO₂)₄ paddlewheel building block is connected by bipy (**1**) or bpe (**2**) organic pillar results 3D α-polonium type frameworks. Framework **1** is rigid and robust without any guest molecules, whereas **2** is flexible, realized by the guest induced structural transformations. Both the frameworks show high thermal stability. Framework **1** and dehydrated form of **2**, i.e. **2'** contains 16.6% and 21.4% void space, respectively and Langmuir surface area calculated from nitrogen adsorption study for **1** and **2'** is 113.0 and 337.5 m²/g, respectively. Both the frameworks can store approximately 1 wt % of molecular hydrogen at 77 K and 15 bar, in particular, the density of adsorbed hydrogen in **1** is one of the highest reported so far in porous MOCPs. Compounds **1** and **2'** can also store 11.0 and 13.2 wt % carbon dioxide at 195 K.

Introduction

After two decades of extensive and authoritative research on metal-organic coordination polymers (MOCPs), the important properties and applications of these materials is unequivocal to the scientific community. Among the various important practical applications, viz., gas

storage, separation, catalysis, and ion exchange,^{1–4} the hydrogen storage presents a serious scientific challenge to the scientists and is still an unsolved problem.⁵ MOCPs are believed to be promising material for hydrogen storage and effort in this regard is continuing to achieve the DOE target.⁶ Recent results by Yaghi et al. suggests that

*To whom correspondence should be addressed. E-mail: tmaji@jncasr.ac.in. Tel: (+91)-80-2208-2826; Fax: (+91)-80-2208-2766.

- (1) (a) Lin, X.; Jia, J.; Zhao, X.; Thomas, K. M.; Blake, A. J.; Walker, G. S.; Champness, N. R.; Hubberstey, P.; Schröder, M. *Angew. Chem., Int. Ed.* **2006**, *45*, 7358. (b) Dincă, M.; Yu, A. F.; Long, J. R. *J. Am. Chem. Soc.* **2006**, *128*, 8904. (c) Ma, S.; Sun, D.; Ambrogio, M.; Fillinger, J. A.; Parkin, S.; Zhou, H.-C. *J. Am. Chem. Soc.* **2007**, *129*, 1858. (d) Dybtsev, D. N.; Chun, H.; Yoon, S. H.; Kim, D.; Kim, K. *J. Am. Chem. Soc.* **2004**, *126*, 32. (e) Matsuda, R.; Kitaura, R.; Kitagawa, S.; Kubota, Y.; Belosludov, R. V.; Kobayashi, T. C.; Sakamoto, H.; Chiba, T.; Takata, M.; Kawazoe, Y.; Mita, Y. *Nature* **2005**, *436*, 238. (f) Dincă, M.; Long, J. R. *J. Am. Chem. Soc.* **2005**, *127*, 9376. (g) Pan, L.; Parker, B.; Huang, X.; Olson, D. H.; Lee, J. Y.; Li, J. *J. Am. Chem. Soc.* **2006**, *128*, 4180. (h) Ma, S.; Sun, D.; Simmons, J. M.; Collier, C. D.; Yuan, D.; Zhou, H.-C. *J. Am. Chem. Soc.* **2008**, *130*, 1012.
- (2) (a) Li, G.; Yu, W.; Ni, J.; Liu, T.; Liu, Y.; Sheng, E.; Cui, Y. *Angew. Chem., Int. Ed.* **2008**, *47*, 1245. (b) Xiong, R.-G.; You, X. *-Zi*; Abrahams, B. F.; Xue, Z.; Che, C.-M. *Angew. Chem., Int. Ed.* **2001**, *40*, 4422. (c) Pan, L.; Olson, D. H.; Ciemnomolowski, L. R.; Heddy, R.; Li, J. *Angew. Chem., Int. Ed.* **2006**, *45*, 616. (d) Chen, B.; Liang, C.; Yang, J.; Contreas, D. S.; Clancy, Y. L.; Lobkovsky, E. B.; Yaghi, O. M.; Dai, S. *Angew. Chem., Int. Ed.* **2006**, *118*, 1418. (e) Liu, H. K.; Sun, W. Y.; Tang, W.-X.; Yamamoto, T.; Ueyama, N. *Inorg. Chem.* **1999**, *38*, 6313. (f) Liu, H. K.; Sun, W. Y.; Ma, D. J.; Yu, K. B.; Tang, W.-X. *Chem. Commun.* **2000**, 591. (g) Maji, T. K.; Matsuda, R.; Kitagawa, S. *Nat. Mater.* **2007**, *6*, 142.

- (3) (a) Guillou, N.; Forster, P. M.; Gao, Q.; Chang, J. S.; Nogues, M.; Park, S.-E.; Cheetham, A. K.; Ferey, G. *Angew. Chem., Int. Ed.* **2001**, *40*, 2831. (b) Horike, S.; Dinca, M.; Tamaki, K.; Long, J. R. *J. Am. Chem. Soc.* **2008**, *130*, 5854. (c) Wu, C. D.; Hu, A.; Zhang, L.; Lin, W. B. *J. Am. Chem. Soc.* **2005**, *127*, 8940. (d) Hasegawa, S.; Horike, S.; Matsuda, R.; Furukawa, S.; Mochizuki, K.; Kinoshita, Y.; Kitagawa, S. *J. Am. Chem. Soc.* **2007**, *129*, 2607. (e) Dybtsev, D. N.; Nuzhdin, A. L.; Chun, H.; Bryliakov, K. P.; Talsi, E. P.; Fedin, V. P.; Kim, K. *Angew. Chem., Int. Ed.* **2006**, *45*, 916. (f) Seo, J. S.; Whang, D.; Lee, H.; Jun, S. I.; Oh, J.; Jeon, Y. J.; Kim, K. *Nature* **2000**, *404*, 982.
- (4) (a) Sun, W. Y.; Fan, J.; Okamura, T.-A.; Xie, J.; Yu, K.-B.; Ueyama, N. *Chem.–Eur. J.* **2001**, *7*, 2557. (b) Fan, J.; Sun, W. Y.; Okamura, T.-A.; Xie, J.; Tang, W.-X.; Okamura, N. *New J. Chem.* **2002**, *26*, 199. (c) Părvulescu, A. N.; Marin, G.; Suwinska, K.; Kravtsov, V. C.; Andruh, M.; Părvulescu, V.; Părvulescu, V. I. *J. Mater. Chem.* **2005**, *15*, 4234. (d) Tzeng, B.-C.; Chiu, T.-H.; Chen, B.-S.; Lee, G.-H. *Chem.–Eur. J.* **2008**, *14*, 5237. (e) Muthu, S.; Yip, J. H. K.; Vittal, J. J. *J. Chem. Soc., Dalton Trans.* **2002**, 4561.
- (5) (a) Schlapbach, L. *MRS Bull.* **2002**, *27*, 675. (b) Schlapbach, L.; Zittel, A. *Nature* **2001**, *414*, 353.
- (6) (a) *National Hydrogen Energy Roadmap*; from the National Hydrogen Energy Roadmap Workshop, Washington D.C., April 2–3, 2002; United States Department of Energy: Washington, D.C., 2002; http://www.eere.energy.gov/hydrogenandfuelcells/pdfs/national_h2_roadmap.pdf. (b) *Hydrogen Posture Plan*; United States Department of Energy: Washington, D.C., 2004; http://www.eere.energy.gov/hydrogenandfuelcells/pdfs/hydrogen_posture_plan.pdf.

microporous MOCPs are able to store hydrogen at a capacity unmatched by other porous materials.⁷ Among the porous materials, MOCPs are potential candidates for hydrogen adsorption and the storage capacity can be enhanced in various ways, e.g., by (a) introducing open metal sites in MOCPs, (b) functionalizing organic linkers, (c) doping of alkali elements onto the organic linker parts of MOCPs, (d) catenation, etc.^{8–11} Strategies such as using pore sizes comparable to hydrogen molecule¹² and introducing coordinatively unsaturated metal centers^{8b,12b,c,13} have been explored. Grand canonical Monte Carlo simulations demonstrate that interpenetration can be beneficial for improving hydrogen storage in MOCPs at cryogenic temperatures.¹⁴ It is believed that favorable interactions exist between hydrogen molecules and porous frameworks composed of the linkers having aromatic rings that have significant influence on hydrogen uptake.¹⁵ Interpenetration can be utilized to further strengthen the interaction between the gaseous molecules and the framework by an entrapment mechanism in which a hydrogen molecule is in proximity with several aromatic rings from interpenetrating frameworks.¹⁶ Zhou et al. have shown that framework interpenetration is one route to derive small pore, whereupon identical frameworks with larger pore interweave to a smaller one, thus increasing stability as well as hydrogen uptake.^{1c,12c,17} Moreover, interpenetrated frameworks are very rigid and they retain porosity even after the loss of guest molecules, thus making them a good choice for studying adsorption properties. Besides framework interpenetration, a computational study by Zhong et al. have shown that the secondary building units (SBUs) formed by metal–oxygen clusters are also preferential adsorption sites for hydrogen.¹⁸ We have combined both these factors, interpenetration as well as paddle-wheel building

unit composed of metal–oxygen cluster in a single framework and have derived two new MOCPs by changing pillar modules. Herein, we report syntheses, structural characterization and adsorption properties of two new MOCPs of Cu(II) $[\text{Cu}_3(\text{bipy})_{1.5}(2,6\text{-ndc})_3]_n$ (**1**) and $\{[\text{Cu}(\text{bpe})_{0.5}(2,6\text{-ndc})] \cdot 0.5\text{H}_2\text{O}\}_n$ (**2**) (4,4'-bipyridine, bipy; 1,2-bis(4-pyridyl)ethane, bpe; 2,6-naphthalenedicarboxylic acid, 2,6-ndc) composed of a mixed-ligand system. Use of 2,6-ndc features a $\text{Cu}_2(\text{CO}_2)_4$ paddlewheel building block and further connection by the long organic linkers, like bipy and bpe, resulting in α -Po type 3D frameworks. Both the frameworks undergo 3-fold interpenetration and exhibit high surface area with good hydrogen and carbon dioxide storage capacity. Structural flexibility is realized by changing the organic linker bipy in **1** to bpe in **2** having a flexible $-(\text{CH}_2)_2-$ unit. Framework **1** exhibits a very high hydrogen density at 77 K reported so far in MOCPs.

Experimental Section

Materials. All the reagents and solvents employed were commercially available and used as supplied without further purification. $\text{Cu}(\text{ClO}_4)_2 \cdot 6\text{H}_2\text{O}$, 2,6-naphthalenedicarboxylic acid, 4,4'-bipyridine and 1,2-bis(4-pyridyl)ethane were obtained from the Aldrich Chemical Co.

Physical Measurements. The elemental analyses were carried out on a Perkin-Elmer 2400 instrument. Thermo gravimetric analyses (TGA) were carried out with a Rigaku Instrument TG8120 in nitrogen atmosphere. IR spectra were recorded on a Bruker IFS 66v/S spectrophotometer with samples prepared in KBr pellets in the region 4000–400 cm^{-1} . X-ray powder diffraction (XRPD) data were collected on a Bruker D8 Discover instrument using Cu $K\alpha$ radiation.

Adsorption Measurements. The adsorption isotherm of nitrogen (77 K) and carbon dioxide (195 K) were measured in the gaseous state by using BELSORP-18-Plus volumetric adsorption equipment from BEL Japan. In the sample chamber (~ 17.5 mL) maintained at $T \pm 0.03$ K was placed the adsorbent sample (~ 100 – 150 mg), which had been prepared at 373 K for **1** and 393 K for **2** under a 1×10^{-1} Pa vacuum for about 6 h prior to measurement of the isotherms. Helium gas at a certain pressure was introduced in the gas chamber and allowed to diffuse into the sample chamber by opening the valve. The change in pressure allowed an accurate determination of the volume of the total gas phase. The amount of gas adsorbed was calculated readily from pressure difference ($P_{\text{cal}} - P_{\text{e}}$), where P_{cal} is the calculated pressure with no guest adsorption and P_{e} is the observed equilibrium pressure. All operations were computer-controlled and automatic. High-pressure hydrogen sorption isotherm measurements at 77 K were carried out on a fully computer controlled volumetric BELSORP-HP, BEL JAPAN high-pressure instrument. The hydrogen used for the high-pressure measurements is scientific/research grade with 99.999% purity. For the measurements, approximately 200 mg of sample was taken in a stainless-steel sample holder and degassed at 373 K for **1** and 393 K for **2** under a 1×10^{-1} Pa vacuum for about 6 h. The dead volume of the sample cell was measured with helium gas of 99.999% purity. Nonideal correction for hydrogen gas was made by applying virial coefficients at the measurement temperature.

Synthesis of $[\text{Cu}_3(\text{bipy})_{1.5}(2,6\text{-napdc})_3]_n$ (1**).** An aqueous solution (50 mL) of $\text{Na}_2\text{-2,6-ndc}$ (1 mmol, 0.260 g) was mixed with

- (7) Rosi, N. L.; Eckert, J.; Eddaoudi, M.; Vodak, D. T.; Kim, J.; O'Keeffe, M.; Yaghi, O. M. *Science* **2003**, *300*, 1127.
- (8) (a) Dinca, M.; Dailly, A.; Liu, Y.; Brown, C. M.; Neumann, D. A.; Long, J. R. *J. Am. Chem. Soc.* **2006**, *128*, 16876. (b) Chen, B.; Ockwig, N. W.; Millward, A. R.; Contreras, D. S.; Yaghi, O. M. *Angew. Chem., Int. Ed.* **2005**, *44*, 4745. (c) Forster, P. M.; Eckert, J.; Chang, J. S.; Park, S. E.; Férey, G.; Cheetham, A. K. *J. Am. Chem. Soc.* **2003**, *125*, 1309.
- (9) (a) Mulfort, K. L.; Hupp, J. T. *J. Am. Chem. Soc.* **2007**, *129*, 9604. (b) Mulfort, K. L.; Hupp, J. T. *Inorg. Chem.* **2008**, *47*, 7936. (c) Rowsell, J. L. C.; Yaghi, O. M. *J. Am. Chem. Soc.* **2006**, *128*, 1304.
- (10) (a) Hüber, O.; Glöss, A.; Fichtner, M.; Klopffer, W. *J. Phys. Chem. A* **2004**, *108*, 3019. (b) Han, S. S.; Goddard III, W. A. *J. Phys. Chem. C* **2008**, *112*, 13431.
- (11) (a) Yaghi, O. M. *Nat. Mater.* **2007**, *6*, 92. (b) Kesanli, B.; Cui, Y.; Smith, M. R.; Bittner, E. W.; Bockrath, B. C.; Lin, W. *Angew. Chem., Int. Ed.* **2005**, *44*, 72. (c) Sun, D.; Ma, S.; Ke, Y.; Collins, D. J.; Zhou, H.-C. *J. Am. Chem. Soc.* **2006**, *128*, 3896.
- (12) (a) Pan, L.; Sander, M. B.; Huang, X.; Li, J.; Smith, M.; Bittner, E.; Bockrath, B.; Johnson, J. K. *J. Am. Chem. Soc.* **2004**, *126*, 1308. (b) Rowsell, J. L. C.; Yaghi, O. M. *Angew. Chem., Int. Ed.* **2005**, *44*, 4670 and references therein. (c) Sun, D.; Ma, S.; Ke, Y.; Collins, D. J.; Zhou, H.-C. *J. Am. Chem. Soc.* **2006**, *128*, 3896.
- (13) Dietzel, P. D. C.; Panella, B.; Hirscher, M.; Blom, R.; Fjellvag, H. *Chem. Commun.* **2006**, 959.
- (14) Ryan, P.; Broadbelt, L. J.; Snurr, R. Q. *Chem. Commun.* **2008**, 4132.
- (15) Ma, S.; Zhou, H.-C. *J. Am. Chem. Soc.* **2006**, *128*, 11734.
- (16) Nechaev, Y. S.; Alexeeva, O. K. *Int. J. Hydrogen Energy* **2003**, *28*, 1433.
- (17) Li, J.; Furuta, T.; Goto, H.; Ohashi, T.; Fujiwara, Y.; Yip, S. *J. Chem. Phys.* **2003**, *119*, 2376.
- (18) Yang, Q.; Zhong, C. *J. Phys. Chem. B* **2006**, *110*, 655.

ethanolic solution (50 mL) of bipy (0.5 mmol, 0.078 g) and the resulting solution was stirred for 20 min to mix well. Cu(CIO₄)₂·6H₂O (1 mmol, 0.370 g) was dissolved in 100 mL of water, and 2 mL of this Cu(II) solution was slowly and carefully layered with the above mixed-ligand solution using 1 mL buffer (1:2 of water and EtOH) solution. Green square-block-shaped crystals were obtained after 1 month. The crystal was separated and washed with an EtOH/water (1:1) mixture and air-dried. (Yield 80%). Anal. Calcd for C₅₁H₃₀Cu₃N₃O₁₂: C, 57.38; H, 2.83; N, 3.94. Found: C, 57.05; H, 2.91; N, 3.68%. FT-IR (KBr pellet, 4000–400 cm⁻¹): 1608(S), 1419(S), 1346(m), 1309(m), 840(m).

Synthesis of {[Cu(bpe)_{0.5}(2,6-napdc)]·(0.5H₂O)}_n (2). Green single crystals of **2** were obtained by following the same procedure of **1**, only changing bpe with bipy. Yield 90%. Anal. Calcd for C₁₈H₁₃CuNO_{4.5}: C, 57.07; H, 3.46; N, 3.70. Found: C, 56.78; H, 3.28; N, 3.56%. FT-IR (KBr pellet, 4000–400 cm⁻¹): 3450 (b, s), 2956 (m), 2875(w), 1608(S), 1419(S), 1346(m), 1309(m), 840(m).

The bulk amounts of both the compounds were synthesized in powder form by the direct mixing of the corresponding ligands solution with aqueous solution of Cu(II). The purity of the samples was confirmed from similarity of XRPD patterns of the bulk phase with the simulated pattern. The compounds were further characterized by IR and elemental analyses.

X-ray Crystal Structure Determination. For each of **1** and **2**, a suitable single crystal was mounted on a glass fiber and coated with epoxy resin and X-ray data was collected on a Rigaku Mercury Diffractometer with graphite monochromated Mo K α radiation ($\lambda = 0.71069$ Å) equipped with a CCD 2D detector. In both cases, the size of the unit cells was calculated from the reflections collected on the setting angles of seven frames by changing of 0.5° for each frame. Three different settings were used and were changed by 0.5° per frame and intensity data were collected with a scan width of 0.5°. Empirical absorption correction by using REQABA was performed in both cases.¹⁹ Structures of **1** and **2** were solved by direct methods using the SIR-97 program²⁰ and expanded using Fourier techniques.²¹ For both the compounds, the non-hydrogen atoms were refined anisotropically (except the oxygen atom (O5) of guest water molecule in **2**, which was refined isotropically) and all hydrogen atoms placed in the ideal positions. All calculations were carried out using SHELXL 97,²² PLATON 99,²³ SHELXS 97,²⁴ and the WinGX system, ver 1.70.01.²⁵ Potential solvent accessible area or void space was calculated using the PLATON²³ multipurpose crystallographic software. All crystallographic and structure refinement parameters are summarized in Table 1. Selected bond lengths and angles for **1** and **2** are displayed in Tables 2 and 3 respectively.

(19) Jacobson, R. A. *REQABA Empirical Absorption Correction*, version 1.1–0301998; Molecular Structure Corp.: The Woodlands, TX, 1996–1998.

(20) Altomare, A.; Burla, M. C.; Camalli, M.; Cascarano, G. L.; Giacovazzo, C.; Guagliardi, A.; Moliterni, A. G. G.; Polidori, G.; Spagna, R. *J. Appl. Crystallogr.* **1999**, *32*, 115.

(21) Beurskens, P. T.; Admiraal, G.; Beurskens, G.; Bosman, W. P.; deGelder, R.; Israel, R.; Smits, J. M. M. *The DIRDIF-94 Program System*; Technical Report of the Crystallography Laboratory; University of Nijmegen: Nijmegen, The Netherlands, 1994.

(22) Sheldrick, G. M., *SHELXL 97, Program for the Solution of Crystal Structure*; University of Göttingen: Göttingen, Germany, 1997.

(23) Spek, A. L. *J. Appl. Crystallogr.* **2003**, *36*, 7.

(24) Sheldrick, G. M. *SHELXS 97, Program for the Solution of Crystal Structure*; University of Göttingen: Göttingen, Germany, 1997.

(25) Farrugia, L. J. *J. Appl. Crystallogr.* **1999**, *32*, 837.

Table 1. Crystal Data and Structure Refinement Parameters for 1 and 2

	1	2
empirical formula	C ₅₁ H ₃₀ Cu ₃ N ₃ O ₁₂	C ₁₈ H ₁₃ CuNO _{4.5}
<i>M</i>	1067.43	378.84
cryst syst	monoclinic	monoclinic
space group	C2 (No. 5)	C2/c (No.15)
<i>a</i> (Å)	17.250(10)	17.094(3)
<i>b</i> (Å)	19.467(9)	19.605(3)
<i>c</i> (Å)	14.031(12)	11.782(2)
α (deg)	90	90.00
β (deg)	95.22(5)	113.950(4)
γ (deg)	90	90.00
<i>V</i> (Å ³)	4692(5)	3608.5(10)
<i>Z</i>	4	8
<i>T</i> (K)	233	243
λ (Mo K α)	0.71073	0.71073
<i>D_c</i> (g cm ⁻³)	1.511	1.391
μ (mm ⁻¹)	1.415	1.233
θ_{\max} (deg)	27.5	27.5
total data	10299	4081
data [<i>I</i> > 2 σ (<i>I</i>)]	8268	2909
<i>R^a</i>	0.0395	0.0576
<i>R_w^b</i>	0.0975	0.1903
GOF	1.04	1.05

$$^a R = \sum |F_o| - |F_c| / \sum |F_o|, \quad ^b R_w = [\sum \{w(F_o^2 - F_c^2)^2\} / \sum \{w(F_o^2)^2\}]^{1/2}.$$

Table 2. Selected Bond lengths (Å) and Angles (deg) for 1

Cu1–O4_c	1.936(5)	Cu1–O3_e	1.940(5)
Cu1–N1	2.174(3)	Cu1–O2_b	1.997(5)
Cu1–O1	1.986(5)	Cu2–O5	1.981(5)
Cu2–O6	1.954(5)	Cu2–N2	2.164(3)
Cu2–O7_k	1.943(6)	Cu2–O8_l	2.003(5)
Cu3–O9	2.004(5)	Cu3–O10	1.940(6)
Cu3–N3_g	2.162(3)	Cu3–O11_k	1.953(5)
Cu3–O12_l	1.969(5)		
O5–Cu2–O6	89.4(2)	O2_b–Cu1–O3_e	168.4(2)
O5–Cu2–N2	97.7(2)	O2_b–Cu1–O4_c	90.8(2)
O5–Cu2–O7_k	168.7(2)	O5–Cu2–O8_l	88.7(2)
O6–Cu2–N2	97.0(2)	O6–Cu2–O7_k	87.9(2)
O6–Cu2–O8_l	166.5(2)	O7_k–Cu2–N2	93.4(2)
O8_l–Cu2–N2	96.5(2)	O7_k–Cu2–O8_l	91.4(2)
O9–Cu3–O10	91.5(2)	O9–Cu3–N3_g	95.3(3)
O9–Cu3–O11_k	166.8(2)	O9–Cu3–O12_l	89.0(2)
O10–Cu3–N3_g	93.4(3)	O10–Cu3–O11_k	87.8(2)
O10–Cu3–O12_l	168.7(2)	O11_k–Cu3–N3_g	97.9(3)
O12_l–Cu3–N3_g	97.8(3)	O11_k–Cu3–O12_l	89.1(2)
O3_e–Cu–O4_c	87.8(2)	O1–Cu1–O2_b	89.1(2)
O1–Cu1–O4_c	167.5(2)	O1–Cu1–O3_e	89.8(2)
O2_b–Cu1–N1	93.6(2)	O4_c–Cu1–N1	95.3(2)
O3_e–Cu1–N1	98.1(2)	O1–Cu1–N1	97.2(2)

Symmetry codes: $b = 1 - x, y, 1 - z$; $c = -1/2 + x, -1/2 + y, z$; $e = 3/2 - x, -1/2 + y, 1 - z$; $g = x, y, -1 + z$; $k = 1/2 + x, -1/2 + y, z$; $l = 1/2 + x, 1/2 + y, z$.

Table 3. Selected Bond lengths (Å) and Angles (deg) for 2

Cu1–O1	1.996(3)	Cu1–N1	2.160(3)
Cu1–O2_a	1.942(3)	Cu1–O3_d	2.000(3)
Cu1–O4_f	1.937(3)		
O1–Cu1–N1	102.03(14)	O1–Cu1–O2_a	88.21(13)
O1–Cu1–O3_d	160.85(13)	O1–Cu1–O4_f	90.18(14)
O2_a–Cu1–N1	93.13(14)	O3_d–Cu1–N1	97.13(14)
O4_f–Cu1–N1	93.82(14)	O2_a–Cu1–O3_d	90.59(14)
O2_a–Cu1–O4_f	173.05(14)	O3_d–Cu1–O4_f	88.72(14)

Symmetry codes: $a = 1 - x, y, 3/2 - z$; $d = -1/2 + x, -1/2 + y, z$; $f = 3/2 - x, -1/2 + y, 3/2 - z$.

Results and Discussion

Structural Description of 1 and 2. X-ray single-crystal structure determination of **1** and **2** reveals a 3D 3-fold interpenetrated framework constructed by Cu(II), 2,6-ndc and pyridyl linkers, bipy in **1** and bpe in **2** respectively.

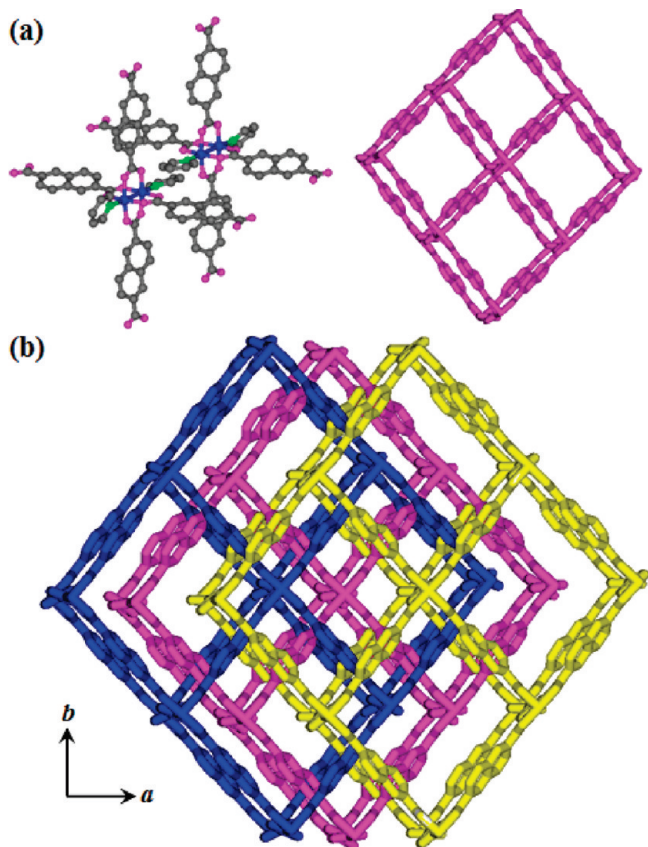


Figure 1. Crystal structure of **1**: (a) left, coordination environment of Cu(II) (copper, blue; oxygen, pink; nitrogen, green; carbon, gray); right, simplistic view of a single net in **1**. (b) 3D view of the α -Po type 3-fold interpenetrated framework along the c direction (hydrogen atoms are removed for clarity).

Essentially, the basic building unit of **1** and **2** is a $\text{Cu}_2(\text{CO}_2)_4$ paddle-wheel core connected by 2,6-ndc leading to a 2D infinite grid in the ab plane. The 2D square grids are further pillared by the pyridyl linkers along c direction resulting 3D frameworks. The overall topology of the frameworks is best described as a compressed primitive cubic α -Po type net. Compound **1** crystallizes in monoclinic system (space group $C2$) with no guest molecules in the lattice. There are three crystallographically independent Cu(II) centers in the asymmetric unit, Cu1, Cu2, and Cu3 (Figure 1a, top left). Structurally, there are three different 3D nets in **1** marked as blue, pink and yellow (Figure 1b) interlocked to each other, but chemically there are two, pink and yellow being the same. Each Cu(II) in each net locates itself in a distorted octahedral geometry with $[\text{CuO}_4\text{NCu}]$ chromophore (Figure 1a). The four coordinations in the equatorial plane is furnished by four oxygen atoms from four different 2,6-ndc while the fifth one at the axial site is provided by a pyridyl nitrogen from bipy. The Cu–Cu bond distance is 2.654 Å, which is similar in all the three nets, fulfills the sixth coordination at the axial site. Because of the longer building units employed (2,6-ndc ≈ 9 Å and bipy ≈ 7 Å), each 3D net houses large 3D channels, (10 Å \times 10 Å, Figure 1a, top right) which facilitates the interlocking of the nets. The 3D framework houses bilateral triangular channels of dimension 3.4×3.1 Å² along crystallographic

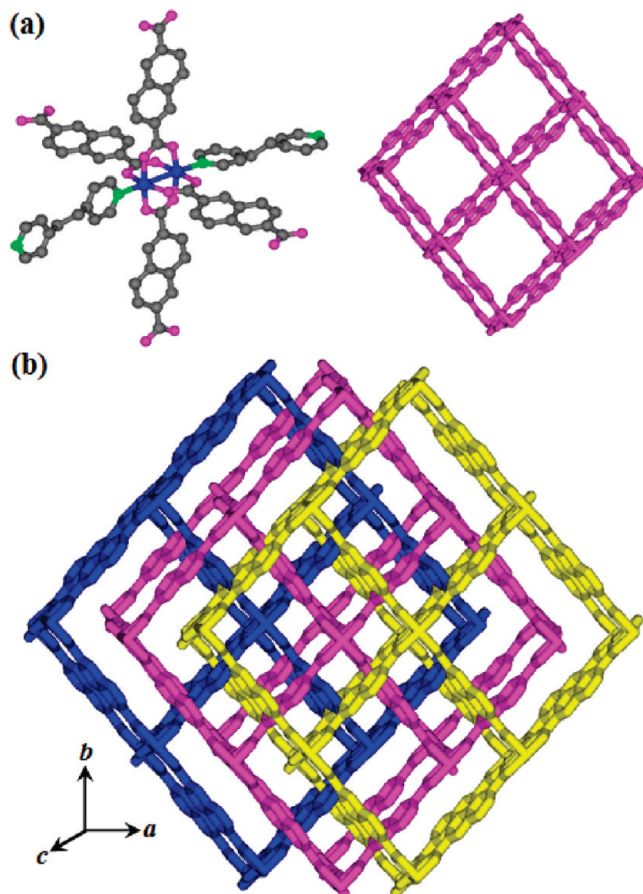


Figure 2. Crystal structure of **2**: (a) left, coordination environment of Cu(II) (copper, blue; oxygen, pink; nitrogen, green; carbon, gray); right, simplistic view of a single net in **2**. (b) 3D view of the α -Po type 3-fold interpenetrated framework (hydrogen atoms and water molecules are removed for clarity).

[101] direction (Figure 3a).²⁶ Calculation using PLATON suggest 16.6% (781 Å³) void volume to the total crystal volume. Cu \cdots Cu separation along Cu \cdots bipy \cdots Cu in two nets are 11.377 and 11.384 Å, respectively. Nearest Cu \cdots Cu separation along Cu \cdots 2,6-ndc \cdots Cu in both the nets is same, 13.005 Å. The difference of blue net with the pink and yellow net is brought out by Cu–O and Cu–N bond lengths, 1.936–1.997 (Cu–O), 2.174 (Cu–N) Å in the blue net and 1.943–2.003 (Cu–O), 2.162–2.164 (Cu–N) Å in the pink and yellow nets, respectively. Compound **2** crystallizes in monoclinic system ($C2/c$). Unlike **1**, there is one Cu(II) center in the asymmetric unit of **2**; however, a basic paddle wheel building unit $\text{Cu}_2(\text{CO}_2)_4$ forms 3D α -Po type framework connected by 2,6-ndc and bpe linker. Because of the longer linker, bpe, employed in **2**, a half of a crystalline water molecule per formula unit could manage its place in the framework even in the presence of 3-fold interpenetration. As in **1**, 3-fold interpenetration in **2** also results because of the presence of three structurally different 3D nets (Figure 2b), but unlike in **1**, the three nets are chemically similar. The coordination environment of Cu(II) in **2** is also defined by a

(26) The sizes of the channels were calculated considering the van der Waals radii of the atoms, and the numbers indicate the median and base of the bilateral triangles.

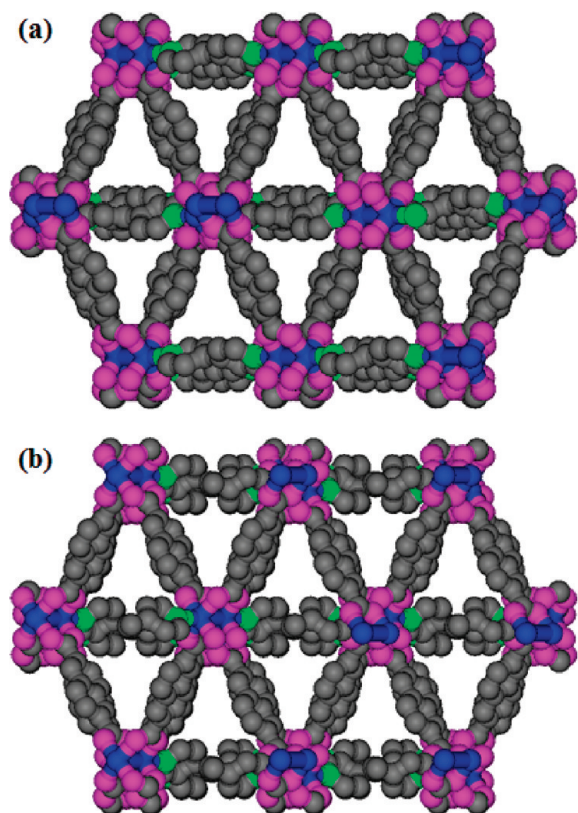


Figure 3. View of the bilateral triangular channels in (a) **1** and (b) **2** along the [101] directions. The channels in **2** are occupied by guest water molecules, whereas in **1**, channels are free.

distorted octahedron with [CuO₄NCu] chromophore (Figure 2a); with N-coordination coming from the bpe pillar. The Cu–Cu bond distance in the paddle wheel is 2.699 Å. The overall framework shows two different type of channels, one bilateral triangular channel along the crystallographic [101] direction occupied by guest water molecules (Figures 3b and S1) and the other is a rectangular channel along *c* direction (see Figure S2 in the Supporting Information). The approximate dimensions of the channels are 3.4 × 3.1 and 5.8 × 2.3 Å², respectively.²⁶ The nearest Cu···Cu separation along Cu···2, 6-ndc···Cu and along Cu···bpe···Cu is 13.005 Å and 13.556 Å respectively. Calculation using PLATON shows that the framework **2** possesses 458 Å³ (12.7%) void volume to the total crystal volume, which increases to 771 Å³ (21.4%) after removal of guest water molecules.

Framework Stability. To study the framework stability of **1** and **2**, thermogravimetric analyses (TGA) and powder X-ray diffraction studies (PXRD) at different temperature were carried out. TGA study of **1** suggests that the framework is stable up to 300 °C without any weight loss and then decomposes to unidentified product (see Figure S3 in the Supporting Information). TGA of **1** also correlates the nonexistence of any guest molecule. TGA of **2** shows a weight loss of 2.43% in the temperature range of 90–120 °C consistent with the presence of guest (0.5) water molecules (calc. 2.37%) and the dehydrated framework (**2'**) is stable up to 330 °C (see Figure S3 in the

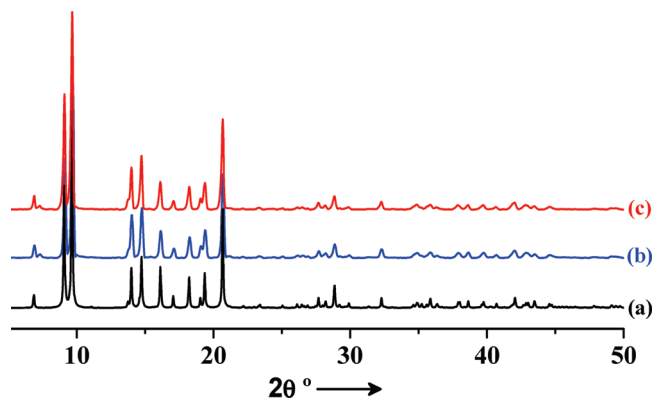


Figure 4. PXRD pattern of **1**: (a) simulated, (b) as-synthesized, and (c) heated at 100 °C for 6 h under a vacuum.

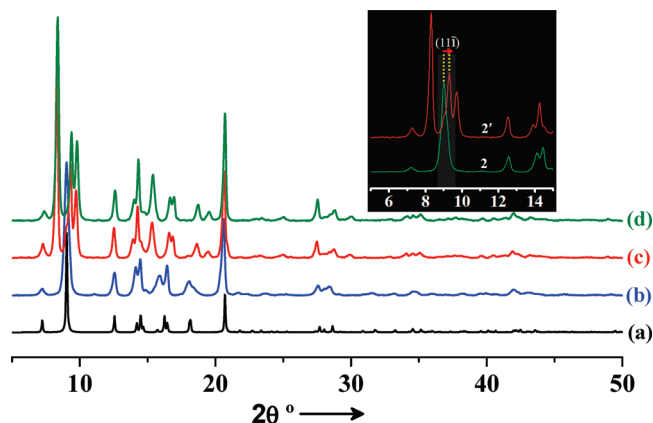


Figure 5. PXRD pattern of **2**: (a) simulated, (b) as-synthesized, (c) heated at 120 °C for 6 h under a vacuum; and (d) rehydrated. Inset diffractogram shows the shifting of (11 $\bar{1}$) peak because of the rearrangement of $-(\text{CH}_2)_2-$ group in **2** after heating at 120 °C.

Supporting Information). Similarity in the PXRD pattern of activated sample of **1** (heated at 100 °C under vacuum) to that of as-synthesized compound is indicative of the fairly rigid and robust framework (Figure 4). However, the dehydrated form of **2**, i.e., **2'**, shows a different pattern with shifting of some peaks and appearance of some new peaks compared to the as-synthesized compound, suggesting structural transformation after removal of the guest water molecules (Figure 5). Indexing of the powder pattern of **2'** by using the TREOR²⁷ program suggests monoclinic crystal system with $a = 16.296(11)$ Å, $b = 21.121(18)$ Å, $c = 11.064(5)$ Å, $\beta = 114.56(5)^\circ$, and $V = 3463.53$ Å³, which indicates the overall contraction of the framework. Most interestingly shrinkage is observed along a and c axis by 4.7 and 6.09% respectively, whereas along the b axis, the structure expands about 7.73%. It is worth mentioning that (11 $\bar{1}$) peak in **2** is shifted to higher angle (9.01 → 9.32) in **2'** and this (11 $\bar{1}$) plane contains flexible $-\text{CH}_2-\text{CH}_2-$ part of the bpe ligand (inset of Figure 5). Therefore, structural transformation in **2** may be realized by the rearrangement of the bpe linker in the (11 $\bar{1}$) plane after the loss of crystalline water molecules (see Figure S4 in the

(27) Werner, P. -E.; Eriksson, L.; Westdahl, M. *J. Appl. Crystallogr.* **1985**, *18*, 367.

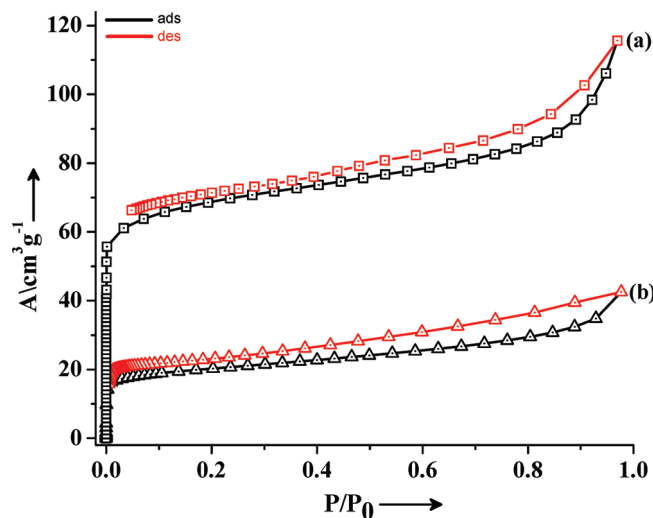


Figure 6. Nitrogen adsorption isotherms recorded at 77 K for (a) **2'** and (b) **1**.

Supporting Information). When **2'** is exposed to water vapor for 3 days, original framework do not regenerates as suggested by the PXRD pattern (Figure 5), indicating irreversible structural transformation.

Adsorption Studies. To study the porous property of the compounds, we subjected **1** and **2'** to nitrogen adsorption analysis. Nitrogen adsorption isotherm at 77 K for both the compounds shows typical type-I behavior with a steep rise at the very low pressure region, suggesting microporous nature of both the frameworks (Figure 6). The volume uptake of nitrogen in **1** and **2'** is 45.5 and 115.6 cm^3/g , respectively. Higher uptake in **2'** is possibly because of larger pore size and greater opening of the pore apertures brought out by the structural rearrangement as evident from the PXRD pattern of **2'**. Langmuir analysis of the isotherms gives surface area of 113 and 337.5 m^2/g for **1** and **2'**, respectively. Small hysteresis in the nitrogen isotherm is probably because of kinetic trapping of adsorbed gas molecules in the cavities having pore openings slightly smaller than the kinetic diameter of the nitrogen molecule. This type of kinetic trapping has been reported by Thomas and co-workers for hydrogen adsorption–desorption isotherms on some MOCPs having flexible organic linkers.²⁸ Interestingly, high-pressure nitrogen adsorption measurement at room temperature shows that nitrogen molecule cannot easily be accommodated in **1**, whereas **2'** shows typical Langmuir type adsorption profile (see Figure S5 in the Supporting Information). The amount adsorbed by **2'** is about three times higher than that of **1**, indicating that the $-(\text{CH}_2)_2-$ group of **2'** make enough space in the channel for smooth access of nitrogen molecules. Realization of the permanent porosity of both the frameworks from nitrogen adsorption study prompted us to analyze the storage capacity of hydrogen and carbon dioxide of **1** and **2'**, and the results are anticipated. The frameworks adsorb

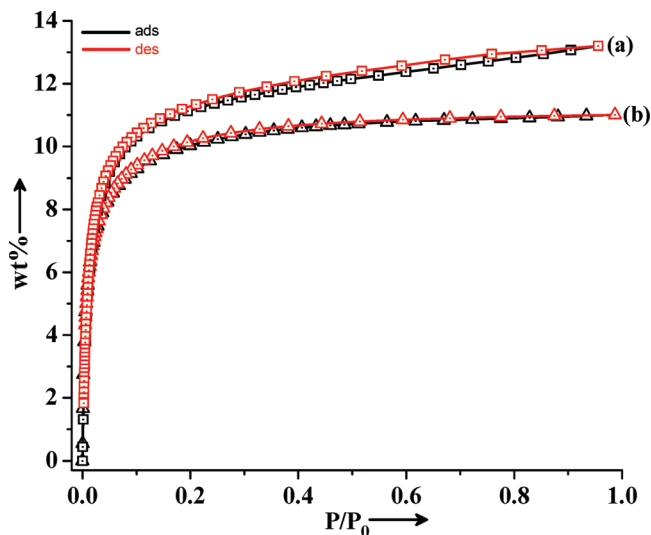


Figure 7. Carbon dioxide adsorption isotherms recorded at 195 K for (a) **2'** and (b) **1**.

significant amount of carbon dioxide, 11 wt % for **1** and 13.2 wt % for **2'** at 195 K (Figure 7). Because the kinetic diameter of carbon dioxide (CO_2 , 3.3 Å) is smaller than the channel dimensions of both the frameworks, the essence of the pore aperture opening in **2'** do not have any significant impact on carbon dioxide uptake and both the frameworks adsorb a comparable volume of the gas. The high value of enthalpy of adsorption, 33.5 kJ/mol for **1** and 31.1 kJ/mol for **2'** indicates strong interaction of carbon dioxide molecules with the pore surface decorated by aromatic rings and $\text{Cu}_2(\text{CO}_2)_4$ core. The most important adsorption result is obtained from hydrogen adsorption study. The hydrogen sorption profile for **1** and **2'** shows a type I curve with steep uptake at the low-pressure region, indicating a strong affinity of hydrogen molecules toward pore surfaces (Figure 8). **1** and **2'** can adsorb 98 cm^3/g (0.88 wt %) and 108 cm^3/g (0.96 wt %) of molecular hydrogen at 15 bar and 77 K. DR analysis of the adsorption isotherms suggests the value of adsorption enthalpy of hydrogen as 3.7 and 4.5 kJ/mol for **1** and **2'**, respectively. These values are within the range of values of adsorption enthalpy of hydrogen reported for many MOCPs. Reported values for adsorption enthalpy of hydrogen on many MOCPs are mostly in the range of 3.5 to 6.5 kJ/mol.^{18,31} The density of the adsorbed hydrogen was calculated based on the pore volume of the frameworks (pore volume, 0.11 cm^3/g for **1** and 0.18 cm^3/g for **2'**), suggesting 0.0801 g/cm^3 for **1** and 0.0611 g/cm^3 for **2'**. The higher value of density of adsorbed hydrogen for **1** compare to liquid hydrogen ($\rho_{\text{H}_2} = 0.0708 \text{ g}/\text{cm}^3$)²⁹ indicates that hydrogen is saturated and highly compressed within the channels of **1**. The high value of hydrogen density can be correlated to the narrow and ordered microchannels in the frameworks.³⁰ The adsorption

(28) Zhao, X.; Xiao, B.; Fletcher, A. J.; Thomas, K. M.; Bradshaw, D.; Rosseinsky, M. J. *Science* **2004**, *306*, 1012. (b) Fletcher, A. J.; Thomas, K. M.; Rosseinsky, M. J. *Solid State Chem.* **2005**, *178*, 2491.

(29) *CRC Handbook of Chemistry and Physics*, 74th ed.; CRC Press: Boca Raton, FL, 1993.

(30) Chun, H.; Dybtsev, D. N.; Kim, H.; Kim, K. *Chem.—Eur. J.* **2005**, *11*, 3521.

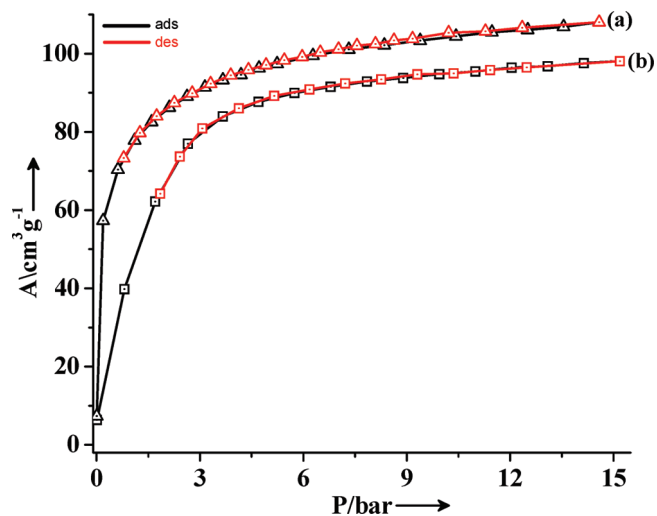


Figure 8. Hydrogen adsorption isotherms for (a) **2'** and (b) **1** measured at 77 K and 15 bar.

isotherm in (a) shows abrupt hydrogen uptake at the low-pressure region compared to that of (b), indicating that the compound **2'** has stronger interaction with hydrogen molecule than compound **1**, which is also reflected in the heat of adsorption values.

We have also checked hydrophilicity of both the frameworks and Figure S6 shows the water sorption profile of **1** and **2'** at 298 K. Framework **1** does not adsorb water molecules up to $P/P_0 = 1$ and type-II sorption profile suggest only surface adsorption (H_2O , kinetic diameter = 2.68 Å). The exclusion of water molecules by **1** is also consistent with the nonexistence of guest water molecules in as-synthesized framework, suggesting hydrophobic nature of the framework. The adsorption profile of **2'** shows gradual increase with pressure and increment is much more prominent at high-pressure regions and ends without saturation at $P/P_0 \approx 1$. A total of ~ 0.6 molecules of water are occluded in framework **2'**. This type of adsorption behavior is attributable to weak affinity for water molecule in **2'**, where adsorbate–adsorbate interactions

also play an important role along with the adsorbent–adsorbate interactions. Moreover, the small uptake in the lower-pressure region is due to the low vapor pressure of the H_2O , and H_2O adsorption phenomenon is always accompanied by the cluster formation in the pore.³²

Conclusion

In conclusion, we have constructed two new triply interpenetrated microporous coordination polymers of Cu(II) using a mixed-ligand system by changing pillar modules from bipy to bpe. The presence of $-(\text{CH}_2)_2-$ groups in the bpe linker induces flexibility in framework **2**. In general, interpenetration is an obstacle to porous functionality in MOCPs; however, **1** and **2** show permanent porosity with interesting hydrogen and carbon dioxide storage capacity. Frameworks **1** and **2'** exhibit high hydrogen storage density; in particular, the density of adsorbed hydrogen in **1** is higher than the liquid hydrogen and is one of the highest values reported so far in porous MOCPs. There are very few reports on multiply interpenetrated robust MOCPs exhibiting hydrogen storage properties. Our results show that small pores are very effective for hydrogen storage as well as for increasing density of the adsorbed hydrogen. A combination of small pore together with large pore volume in a single MOCP might fulfill the requirement of the DOE in the near future.

Acknowledgment. T.K.M. gratefully acknowledges the financial support from DST, Government of India (Fast Track Proposal). P.K. acknowledges CSIR, Government of India, for a senior research fellowship. The authors thank Dr. Golam Mostafa for helpful discussions.

Supporting Information Available: Crystallographic data (CIF); extensive figures and thermogravimetric analysis (PDF). This material is available free of charge via the Internet at <http://pubs.acs.org>.

(31) (a) Bordiga, S.; Vitillo, J. G.; Ricchiardi, G.; Regli, L.; Cocina, D.; Zecchina, A.; Arstad, B.; Bjørgen, M.; Hafizovic, J.; Lillerud, K. P. *J. Phys. Chem. B* **2005**, *109*, 18237. (b) Frost, H.; Düren, T.; Snurr, R. Q. *J. Phys. Chem. B* **2006**, *110*, 9565. (c) Lee, J. Y.; Li, J.; Jagiello, J. *J. Solid State Chem.* **2005**, *178*, 2527.

(32) (a) Bekyarova, E.; Hanzawa, Y.; Kaneko, K.; Silvestre-Albero, J.; Sepulveda-Escribano, A.; Rodriguez-Reinoso, F.; Kasuya, D.; Yudasaka, M.; Iijima, S. *Chem. Phys. Lett.* **2002**, *366*, 463. (b) Kaneko, K.; Hanzawa, Y.; Iiyama, T.; Kanda, T.; Suzuki, T. *Adsorption* **1999**, *5*, 7. (c) Li, D.; Kaneko, K. *Chem. Phys. Lett.* **2001**, *335*, 50. (d) Ohba, T.; Kanoh, H.; Kaneko, K. *Chem.–Eur. J.* **2005**, *11*, 4890.